ION-MOLECULAR REACTIONS WITH ORGANIC AND ATMOSPHERIC COMPOUNDS FROM 150-1400K

Anthony Midey

Northeast Consortium for Engineering Education
68 Port Royal Square
Port Royal, VA 22535
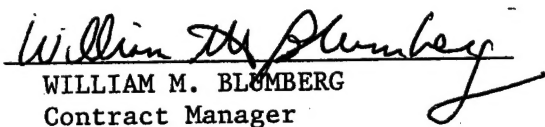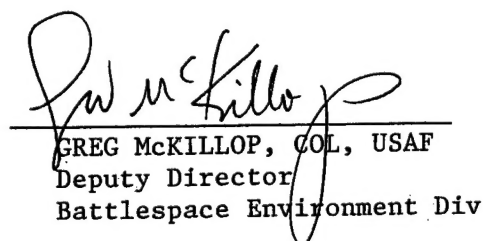
June 2000

Scientific Report

AIR FORCE RESEARCH LABORATORY
Space Vehicles Directorate
29 Randolph Road
AIR FORCE MATERIEL COMMAND
HANSCOM AIR FORCE BASE MA 01731-3010

20020816 073

"This technical report has been reviewed and is approved for publication"

WILLIAM M. BLOMBERG
Contract Manager

GREG McKILLOP, COL, USAF
Deputy Director
Battlespace Environment Div

This report has been reviewed by the ESC Public Affairs Office (PA) and is releasable to the National Technical Information Service (NTIS).

Qualified requestors may obtain additional copies from the Defense Technical Information Center (DTIC). All others should apply to the National Technical Information Service (NTIS).

If your address has changed, if you wish to be removed from the mailing list, or if the addressee is no longer employed by your organization, please notify AFRL/VSIM, 29 Randolph Road, Hanscom AFB MA 01731-3010. This will assist us in maintaining a current mailing list.

Do not return copies of this report unless contractual obligations or notices on a specific document require that it be returned.

REPORT DOCUMENTATION PAGE

1. REPORT DATE (DD-MM-YYYY)	2. REPORT TYPE	3. DATES COVERED (From - To)
22 Jun 2000	Interim	

4. TITLE AND SUBTITLE

Ion-Molecule Reactions with Organic and Atmospheric Compounds from 150-1400 K

5a. CONTRACT NUMBER
F19628-98-C-0029

5b. GRANT NUMBER

5c. PROGRAM ELEMENT NUMBER
62101F

6. AUTHOR(S)

Anthony Midey

5d. PROJECT NUMBER
9993

5e. TASK NUMBER
GS

5f. WORK UNIT NUMBER
PE

7. PERFORMING ORGANIZATION NAME(S) AND ADDRESS(ES)

Northeast Consortium for Engineering Education, 68 Port Royal Square, Port Royal, VA 22535

8. PERFORMING ORGANIZATION REPORT NUMBER

9. SPONSORING / MONITORING AGENCY NAME(S) AND ADDRESS(ES)

Air Force Research Laboratory/VSB
29 Randolph Road
Hanscom AFB MA 01731-3010

10. SPONSOR/MONITOR'S ACRONYM(S)

11. SPONSOR/MONITOR'S REPORT NUMBER(S)

AFRL-VS-TR-2002-1591

12. DISTRIBUTION / AVAILABILITY STATEMENT

Approved for public release: distribution unlimited

13. SUPPLEMENTARY NOTES

14. ABSTRACT

A variable temperature-selected ion flow drift tube (VT-SIFDT) and a high temperature flowing afterglow (HTFA) have been used to study ion-molecule reactions in the 220 - 1400 K temperature range. The effects of electronic, vibrational, and rotational energy on the kinetics of a wide range of reactions important in combustion chemistry have been investigated.

15. SUBJECT TERMS

Phillips Laboratory Scholar Program, variable temperature-selected ion flow draft tube, high temperature flowing afterglow, ion-molecule ractions, combustion chemistry

16. SECURITY CLASSIFICATION OF:			17. LIMITATION OF ABSTRACT	18. NUMBER OF PAGES	19a. NAME OF RESPONSIBLE PERSON
a. REPORT	**b. ABSTRACT**	**c. THIS PAGE**	unlimted	25	WILLIAM A.M. BLUMBERG
unclassfied	unclassified	unclassified			**19b. TELEPHONE NUMBER (include area code)** 781-377-3601

Final Report

Anthony J. Midey, Jr.

NCEE Prime Contract -0029 from 23 June 1999 to 22 June 2000

During the aforementioned contract period, I have employed a variable temperature-selected ion flow drift tube (VT-SIFDT) and a high temperature flowing afterglow (HTFA) to study ion-molecule reactions from 220-1400 K. I have investigated the effects of electronic, translational, rotational and vibrational energy on the kinetics of these reactions. This work has been conducted under the direction of Dr. Albert A. Viggiano at the Air Force Research Laboratory (AFRL) in the Space Vehicles Directorate (VSBP) at Hanscom AFB, MA.

Plasma chemistry occurring at very high temperatures critically impacts Air Force systems. Plasmas can develop around re-entry vehicles that interfere with communications. In addition, the chemistry of the ionosphere occurs at temperatures upwards of 2000 K. Consequently, accurate modeling of ionospheric processes requires measurements of reactions at high temperatures.[1] The HTFA has been designed[2] and used to address these issues.[1, 3, 4] However, weakly ionized systems are also of interest and are readily studied using the VT-SIFDT.

Understanding high temperature ion-molecule chemistry also facilitates the design of airbreathing hypersonic vehicle combustors where the ion chemistry may enhance hydrocarbon fuel combustion.[5] Unfortunately, ion chemistry may also contribute to soot formation in hydrocarbon combustion.[6, 7] Nevertheless, the first step in establishing this technology is modeling the chemistry occurring. However, only neutral molecule chemistry has been included in recent models of soot generation.[8] Accurate models of these processes thus require high temperature data for ion-molecule reactions with many different hydrocarbons, including alkylbenzenes which comprise about 25% by volume of standard jet fuels. The previously mentioned HTFA apparatus has subsequently been employed to address these problems. Recent modifications to the HTFA have expanded its capabilities, allowing measurements of

1

ion-molecule branching ratios at temperatures over 700 K.[9-11] The VT-SIFDT and the HTFA combined permit branching ratios and rate constants to be measured from 85 to 1800 K at pressures from up to 2 torr and kinetic energies up to 1 eV.

The VT-SIFDT operates in the following manner.[12] Ions are generated in a high pressure source region using electron impact on a source gas. The desired reactant ion is mass selected by a quadrupole mass spectrometer and injected into the flow tube. The ions are entrained in a fast flow of helium buffer gas and thermally equilibrate to the flow tube temperature, which is controlled by a combination of heating elements and cooling lines. After thermal equilibration, the neutral reactant is introduced. The residual reactant ions and all product ions are sampled with an orifice and are mass selected by another quadrupole mass spectrometer then detected. For a given temperature, the rate constants are obtained using the decline of the reactant ion signal over a previously measured reaction time as a function of excess neutral reagent concentration where the average center-of-mass kinetic energy is given by:[13]

$$\langle KE_{cm} \rangle = \frac{(m_i + m_b)m_n}{2(m_i + m_n)} + \frac{3}{2}k_B T \tag{1}$$

In Eq. 1, m_i, m_b and m_n are the reactant ion, buffer gas and reactant neutral masses, respectively. The drift tube consists of a series of concentric rings to which a voltage is applied to accelerate the reactant ions to a kinetic energy above the thermal value described by the second term in Eq. 1. The first term above gives the drift tube contribution to the total kinetic energy. Operating the drift tube with no voltage applied allows the instrument to be run as a VT-SIFT. Pseudo-first order kinetics hold under all of these conditions and the rate constants are easily calculated. The branching ratios are measured in two steps to minimize mass discrimination in the mass spectrometer and to allow accurate determination of the individual reaction channels that can differ by only one mass unit. Relative errors in the rate constants are ±15% and the absolute errors are ±25%, while the relative errors in the branching ratios are ±25%.[12]

Rate constants and branching ratios are measured in the HTFA in a similar manner,[2] with a few exceptions. The HTFA has no source selection. Consequently, branching ratios can be measured only for ions that can be generated with large flows of source gas because the ions arise from interaction with high-energy helium species

2

formed in the source region. These large flows guarantee that all unwanted reactive species are consumed before the neutral reagent gas is introduced. Corrections must also be made to the branching ratios for reactive species formed in the flow tube of the HTFA (e.g., N_4^+ when making N_2^+ ions). The uncertainties in the HTFA data[2, 9] are similar to those in the VT-SIFDT.

The rate constants and branching ratios for the reaction of $H_3O^+(H_2O)_n$ clusters with aldehydes CH_2O and CH_3CHO have been studied from 150-294 K with n=0-5 and 200-294 K with n=0-4 in the VT-SIFDT. These measurements address assumptions by Yu et al.[14] that all of the aldehydes that have been used to model ultrafine aerosol formation in jet exhaust from the interaction of charged particles with volatile organic compounds. The current experiments also improve upon previous flowing afterglow measurements where both H_2O and the aldehyde are in the flow tube which means that the system is in equilibrium.[15, 16]

The current results are given in Tables 1 and 2 for CH_3CHO and CH_2O. The CH_3CHO reactions proceed at the collision rate at both temperatures for n=0-4 with ligand switching predominating for n=1-4. The bare H_3O^+ ion reacts via proton transfer. Higher order ligand-switching products from secondary reactions are also observed. The CH_2O reactions show similar products, but the rate constants are both size and temperature dependent. H_3O^+ again reacts by proton transfer at the collision rate at all temperatures in agreement with previous flowing afterglow studies.[16]   The n=1 cluster undergoes ligand switching at around 75% of the collision rate at all temperatures. The n=2 cluster has a negative temperature dependence in the rate constant, probably because of the small association channel present at 150 K. The chemistry of the n=3 and higher clusters is more complex. The rates continue decreasing with increasing cluster size. As seen in Fig. 1 illustrates where the reaction efficiency given by the ratio of the observed rate constant to the collision rate constant is plotted as a function of temperature and cluster size, the largest cluster observed at each temperature shows an anomalous increase. The deviation occurs where the largest cluster is only marginally stable[17, 18] and may be thermally decomposing. However, this would affect the rate constant of the next smallest cluster which is unaffected by the presence of larger clusters in the flow tube. The presence of the association channel does not

account for these results because it is present for n=2 which has a more typical temperature dependence for a system involving an endothermic ligand switching reaction with an association channel at low temperature. The results for CH_2O show that the rate constants for this reaction used by Yu et al.[14] are too large.[19]

To investigate the statistical nature of S_N2 substitution reactions for weakly ionized plasmas, the reactions Cl^- with C_2H_5Br and n-C_3H_7Br have been studied as a function of kinetic energy and temperature in the VT-SIFDT from 220-500 K. For Cl^- reacting with C_2H_5Br, the S_N2 reaction path to give Br^- dominates at all temperatures and kinetic energies. However, an association channel accounts for 5% of the products at 298 K independent of kinetic energy and disappears at 500 K, but it makes a larger contribution at 220 K showing a negative kinetic energy dependence. The rate constants also show a negative kinetic energy dependence and are slightly faster than the corresponding pure temperature data. Fig. 2 shows the total and S_N2 only rate constants as a function of kinetic energy, along with previous experimental measurements.[20-22] The rate constant for the S_N2 reaction only is obtained by multiplying the S_N2 branching fraction by the total rate constant. Comparing the data at different temperatures with the same kinetic energy reveals that the internal temperature does not have a strong influence on the rate constants.

Similar trends arise for the reaction of Cl^- with n-C_3H_7Br, where the S_N2 channel again predominates. The results are given in Fig. 3 along with a previous result.[20] The rate constants are essentially independent of temperature and kinetic energy from 298 to 500 K, again showing a 5% association product channel only at 298 K. The trend indicates that the reaction has no substantial dependence on internal energy. However, a factor of 4 increase in the rate constant at zero drift field at 230 K occurs and the rate constants at kinetic energies up to 0.07 eV decrease with increasing kinetic energy. The higher kinetic energy data are only slightly larger than the values at higher temperatures. The association channel accounts for 35% of the products at zero drift field and decreases to 30% at 0.07 eV at 200 K. A second mechanism involving association followed by dissociation to Br^- and Cl^- via collisions with He buffer gas has been examined by selectively scavenging the association product via secondary

4

reaction with HCl. The results confirm that this mechanism occurs in addition to the direct S_N2 reaction for n-C_3H_7Br.

A similar test with C_2H_5Br displays analogous results, although of smaller magnitude. The energetics of the reactions with both alkylbromides are similar as well and it appears that the importance of the thermal association and dissociation mechanism depends on a balance between the well depth, barrier height and/or the number of degrees of freedom. Based on the presence of the association channel, previous work with S_N2 reactions with association channels,[23, 24] and a weak internal and translational energy dependence, the reactions of Cl⁻ with C_2H_5Br and n-C_3H_7Br should behave statistically.[25] This finding is in contrast to previous work with CH_3Br that indicates the reaction is not statistical.[26-29]

Two reactions that have been studied to high temperatures are N_2^+ with CO_2 and SO_2, which are minor reactions in the atmosphere.[30-32] The reaction of N_2^+ with CO_2 has been studied as a function of temperature from 300-1400 K in the HTFA and kinetic energy from 0.04-0.27 eV in the VT-SIFDT at 298 K. Fig. 4 shows the rate constants plotted vs. the average total energy given by Eq. 2 for a temperature T:

$$\langle Total\ Energy \rangle = RE_{ion} + \langle KE \rangle + \langle E_{int}^{ion} \rangle + \langle E_{int}^{neutral} \rangle \tag{2}$$

where RE_{ion} is the recombination energy of the reactant ion. The average kinetic energy, $\langle KE \rangle$, is determined by Eq. 1 in the VT-SIFDT or by simply $3/2 k_B T$ in the HTFA. The average internal energies of the reactant ion, $\langle E_{int}^{ion} \rangle$, and neutral, $\langle E_{int}^{neutral} \rangle$, include an average rotational energy of $n/2 k_B T$ where n is the number of rotational degrees of freedom and an ensemble average over a Boltzmann distribution of vibrational energy levels for all modes in the harmonic approximation. Zero point energy is neglected in all cases. The effective temperature in the drift tube experiments used to evaluate Eq. 2 is determined by Eq. 1 with $m_n = m_b$.

For N_2^+ with CO_2, the rate constant at 298 K with no drift voltage agrees with those from the HTFA and previous experiments,[33-36] proceeding close to the Langevin collision rate constant. The rate constants decrease with increasing energy, indicating the reaction proceeds through a collision complex as supported by previous work.[37, 38] However, the HTFA results that reflect are larger fraction of internal energy are

consistently lower than the VT-SIFDT results with most translational excitation. Internal energy thus hinders the reactivity relative to translational energy. These results contrast with the results for the energetically similar Ar^+ reaction with CO_2 at high temperatures. In that experiment, the rate constants in the HTFA[39] and a flow drift tube (FDT)[40] agree when plotted vs. total energy up to 0.4 eV. Above this energy, the rate constants in the HTFA are lower than the FDT values. This energy corresponds to the bond energy of the $(Ar \cdot CO_2)^+$ complex which may interfere with the charge transfer reaction. The complex should have similar energy with N_2^+; however, the biggest difference is the rotational excitation of the N_2^+ ion not present with Ar^+.

The reaction of N_2^+ with SO_2 has also been examined in the HTFA up to 1400 K. Fig. 5 shows the rate constants plotted vs. the average total energy. The FDT results of Dotan et al. are also shown, converted to total energy using an effective temperature derived from Eq. 1 as described above. The rate constants agree within the error of the two experiments up to 0.4 eV. The FDT rate constants increase above 0.6 eV where an endothermic dissociative charge transfer channel to give SO^+ is accessible. Fig. 6 shows the rate constants for the individual product channels in both experiments. The rate constant for generating SO^+ increases rapidly when the SO^+ product can be formed, but the trends in the two instruments seem to differ. However, if the data is replotted as the ratio of the SO^+ channel's rate constant to the maximum possible rate constant for reaction from N_2^+ ($v>0$), then the two data sets concur within the scatter. Consequently, the enhancement in the rates is due to producing SO^+ from vibrationally excited states of N_2^+ as seen in previous work.[41] With Ar^+ and SO_2, the vibrational excitation in SO_2 at elevated temperatures enhances the rate constants;[39] however, this enhancement may occur with N_2^+ in a region where the effect of the $N_2^+(v>0)$ states dominates.[42]

To address the needs of the aforementioned combustion models, the kinetics of the reactions of air plasma ions with toluene, ethylbenzene and propylbenzene have been studied in the VT-SIFT from 298-500 K. Other ions with recombination energies between 9 and 16 eV have also been studied at 298 K in the VT-SIFT to construct breakdown curves for the dependence of the branching fractions on predominately electronic energy. These curves allow comparisons with photodissociation

experiments.[43] In addition, the reactions of NO^+ and O_2^+ with all three alkylbenzenes have been studied up to 1400 K in the HTFA. Comparing the results from the two instruments reveals how the larger fraction of internal energy in the high temperature experiments affects the reactivity relative to the mostly electronic excitation in the VT-SIFT. Table 3 shows the rate constants for the air plasma cation reactions at 298 K. All reactions proceed at the Su-Chesnavich collision rate constant for all ions,[44, 45] including those not shown in the table. The rate constants for the NO^+ and O_2^+ ions are independent of temperature to 1400 K, consistent with reactions that proceed at the collision rate.[9, 10]

The breakdown curves for toluene, ethylbenzene and propylbenzene are shown in Figs. 8-10. The branching ratios are plotted against the average total energy calculated using Eq. 2. To examine the effect of the charge-transfer product ion's lifetime on the branching ratios, the flow tube studies have been compared to guided-ion beam (GIB) results that have been conducted at a few orders of magnitude lower pressure. Previous experiments have shown how collisional stabilization of a long-lived energized charge-transfer complex by the buffer gas in the flow tube can affect the observed dissociation thresholds,[9, 10] warranting the low pressure studies. The GIB is equipped with a high temperature octopole[46, 47] (HT8P) that allows cross sections and branching fractions to be measured as a function of both temperature (i.e., internal energy content) and kinetic energy up to 10 eV. The GIB data are also shown in Figs. 8-10 labeled as HT8P, taken at 298 and 650 K.

Comparing the flow tube results in Fig. 8 for toluene, the HTFA and SIFT results agree except for the reaction of NO+ in the HTFA, indicating that rotational and vibrational excitation of the neutral reagent affects the reactivity the same as electronic energy. However, the HT8P results indicate that translational energy is not as efficient at promoting fragmentation. The NO^+ data show a fall-off in the $C_7H_8^+$ branching fraction at the thermochemical threshold for $C_7H_7^+$ formation. Collisions with the He buffer gas cause dissociation of the charge-transfer product, as evidenced by a lack of such behavior at similar energies in the HT8P at low pressures. However, this behavior has been observed previously in the flow tube with $C_8H_{17}^+$ formed from isobutane.[48] Over 85% of the dissociation products are $C_7H_7^+$ in equal amounts of the benzylium and

7

tropylium isomer as determined in a previous VT-SIFT study.[49] The branching ratios for this product are given in the lower panel of Fig. 8.

The observed onset of dissociative charge-transfer with toluene in the flow tube experiments occurs 1 eV higher than the thermochemical threshold.[50] The $C_7H_8^+$ ion lifetime is such that an extra 0.5 eV of energy must be added to get the molecule to fall apart on the timescale for observation in the flow tube, creating a kinetic shift. However, the threshold is shifted another 0.5 eV higher because collisions with the He buffer stabilize the energized charge-transfer product ion. Similar trends have been seen in flow tube studies of benzene and naphthalene to 1400 K.[9, 10]

The analogous breakdown curves for ethylbenzene are shown in Fig. 9. The NO^+ reaction in the HTFA again shows the unusual trend in the $C_8H_{10}^+$ branching fraction caused by dissociation induced through collisions with the He buffer. The fall-off occurs at the thermochemical threshold and is not observed in the HT8P work at similar energy but lower pressure. The O_2^+ data from the HTFA agree well with the VT-SIFDT data intimating that rotational, vibrational and electronic energy are equivalent. Based on the HT8P results, kinetic energy is not as efficient with ethylbenzene. However, it is more efficient than it is for toluene. The lower panel in Fig. 9 shows that over 90% of the dissociation products are $C_7H_7^+$ of which 70% is in the benzylium structure.[49] The better agreement between the low kinetic energy data from the HT8P and the flow tube data at 1 Torr pressure indicates that less of a kinetic shift and collisional stabilization occur. This trend is consistent with deuterium isotope experiments that show that the lifetime of the energized $C_8H_{10}^+$ charge-transfer product ion is shorter than that for toluene.[51]

Fig. 10 shows the breakdown curves for propylbenzene. As with the other reactants, the charge-transfer product ions from NO^+ reaction in the HTFA undergo dissociation via collisions with the He buffer at higher temperatures. Rovibrational and electronic energy affect the reactivity identically and kinetic energy is the most efficient with propylbenzene. Approximately 90% of the products in the lower panel of Fig. 10 are $C_7H_7^+$, of which 90% is in the benzylium form.[49] The flow tube data at 1 Torr pressure and HT8P kinetic energy data at 10^{-4} Torr have even better agreement than

with ethylbenzene at low energies, consistent with the shorter lifetime of the $C_9H_{12}^+$ energized ion.[52]

The data from the combined experiments provides insight into the charge-transfer dynamics for alkylbenzene reactions with air plasma ions. At low kinetic energies, the rate constants proceed at the collision rate. Also, internal and electronic energy behave similarly, together indicating that complex formation occurs. However, kinetic energy is not equivalent to the other forms of energy; therefore, complex formation does not completely describe the mechanism. The reduced efficiency of kinetic energy implies that long-range charge-transfer processes occur at distances where little kinetic energy is exchanged. At higher kinetic energy, the threshold behavior of NO^+ reacting with ethylbenzene and propylbenzene in the HT8P is similar to line-of-centers functions that describe collision induced dissociation (CID) cross sections.[53] These CID cross sections peak at a value approaching the effective hard sphere cross section. The different maximum amounts of fragmentation with O_2^+ and NO^+ in the HT8P may arise from differences in the hard sphere cross sections. However, the asymptotic amounts of dissociation also depend on the initial total energy available. Therefore, near-resonant processes may also occur.[11]

The ion-molecule chemistry of weakly charged plasmas and high temperature environments has been explored using the fast flow tube methods available at the Space Vehicles Directorate of AFRL at Hanscom AFB. The unique capabilities provide comprehensive coverage over the range of operating temperatures found in Air Force systems. A temperature variable version of a recently constructed turbulent ion flow tube[54] (TIFT) will expand these capabilities to afford examining the effects of pressure and temperature on ion-molecule chemistry. It is this adaptability which will allow these powerful techniques to address critical issues for the understanding of basic processes influencing crucial Air Force systems.

REFERENCES

1. P. M. Hierl, I. Dotan, J. V. Seeley, J. M. Van Doren, R. A. Morris and A. A. Viggiano, J. Chem. Phys. **106**, 3540-3544 (1997).

2. P. M. Hierl, J. F. Friedman, T. M. Miller, I. Dotan, M. Mendendez-Barreto, J. Seeley, J. S. Williamson, F. Dale, P. L. Mundis, R. A. Morris, J. F. Paulson and A. A. Viggiano, Rev. Sci. Inst. **67**, 2142 (1996).

3. I. Dotan, P. M. Hierl, R. A. Morris and A. A. Viggiano, Int. J. Mass Spectrom. Ion Phys. **167/168**, 223-230 (1997).

4. I. Dotan and A. A. Viggiano, J. Chem. Phys. **110**, 4730 (1999).

5. S. Williams, S. T. Arnold, P. M. Bench, A. A. Viggiano, I. Dotan, A. J. Midey, T. Morris, R. A. Morris, L. Q. Maurice and E. A. Sutton, 14th International Symposium on Air Breathing Engines, 1999, p.

6. P. Gerhardt and K.-H. Homann, J. Phys. Chem. **94**, 5381 (1990).

7. P. Weilmunster, A. Keller and K.-H. Homann, Combust. Flame **116**, 62 (1999).

8. L. Q. Maurice, T. Edwards and R. C. Striebich, AIAA/ASME/SAE/ASEE 34th Joint Propulsion Conference, 1998, p. AIAA 98-3534.

9. S. T. Arnold, S. Williams, I. Dotan, A. J. Midey, R. A. Morris and A. A. Viggiano, J. Phys. Chem. A **103**, 8421 (1999).

10. A. J. Midey, S. Williams, S. T. Arnold, I. Dotan, R. A. Morris and A. A. Viggiano, Int. J. Mass Spectrom. **195**, 327 (2000).

11. S. Williams, A. J. Midey, S. T. Arnold, R. A. Morris, A. A. Viggiano, Y.-H. chiu, D. J. Levandier, R. A. Dressler and M. R. Berman, J. Phys. Chem. A In press, (2000).

12. A. A. Viggiano, R. A. Morris, F. Dale, J. F. Paulson, K. Giles, D. Smith and T. Su, J. Chem. Phys. **93**, 1149-1157 (1990).

13. G. H. Wannier, Bell. Syst. Tech. J. **32**, 170 (1953).

14. F. Yu, R. P. Turco and B. Kärcher, J. Geophys. Res. **104**, 4079-4087 (1999).

15. F. C. Fehsenfeld, I. Dotan, D. L. Albritton, C. J. Howard and E. E. Ferguson, J. Geophys. Res **83**, 1333 (1978).

16. D. K. Bohme, G. I. Mackay and S. D. Tanner, J. Am. Chem. Soc. **101**, 3724 (1979).

17. Y. K. Lau, S. Ikuta and P. Kebarle, J. Am. Chem. Soc. **104**, 1462-1469 (1982).

18. A. A. Viggiano, F. Dale and J. F. Paulson, J. Chem. Phys. **88**, 2469 (1988).

19. A. J. Midey, S. T. Arnold and A. A. Viggiano, J. Phys. Chem. A **104**, 2706 (2000).

20. C. H. DePuy, S. Gronert, A. Mullin and V. M. Bierbaum, J. Am. Chem. Soc. **112**, 8650 (1990).

21. G. Caldwell, T. F. Magnera and P. Kebarle, J. Am. Chem. Soc. **106**, 959-966 (1984).

22. W. B. Knighton, J. A. Bognar, P. M. O'Conner and E. P. Grimsrud, J. Am. Chem. Soc. **115**, 12079 (1993).

23. R. A. Morris and A. A. Viggiano, J. Phys. Chem. **98**, 3740 (1994).

24. A. A. Viggiano, R. A. Morris, T. Su, B. D. Wladkowski, S. L. Craig, M. Zhong and J. I. Brauman, J. Am. Chem. Soc. **116**, 2213 (1994).

25. A. A. Viggiano and A. J. Midey, J. Phys. Chem. A In press (2000).

26. S. Raugei, G. Cardini and V. Schettino, J. Chem. Phys. **111**, 10887 (1999).

27. S. L. Craig, M. Zhong and J. I. Brauman, J. Am. Chem. Soc. **121**, 11790-11797 (1999).

28. S. Schmatz and D. C. Clary, J. Chem. Phys. **110**, 9483 (1999).

29. W. L. Wang, G. H. Peslherbe and W. L. Hase, J. Am. Chem. Soc. **116**, 9644 (1994).

30. A. S. Jursa, *Handbook of Geophysics and the Space Environment* (NTIS, Springfield VA, 1985).

31. A. A. Viggiano, Mass Spec. Rev. **12**, 115-137 (1993).

32. D. Smith and P. Spanel, Mass Spectrom. Rev. **14**, 255-278 (1995).

33. W. T. Huntress Jr., M. J. McEwan, Z. Karpas and V. G. Anicich, Ap. J. Suppl. Ser. **44**, 481 (1980).

34. F. C. Fehsenfeld, A. L. Schmeltekopf and E. E. Ferguson, J. Chem. Phys. **44**, 4537 (1966).

35. D. Smith, N. G. Adams and T. M. Miller, J. Chem. Phys. **69**, 308 (1978).

36. M. Tichy, A. B. Rakshit, D. G. Lister, N. D. Twiddy, N. G. Adams and D. Smith, Int J. Mass Spectrom. Ion Phys. **29**, 231-247 (1979).

37. D. C. Parent, R. Derai, G. Mauclaire, M. Heninger, R. Marx, M. E. Rincon, A. O'Keefe and M. T. Bowers, Chem. Phys. Lett. **117**, 127-131 (1985).

38. J. A. Gardner, R. A. Dressler, R. H. Salter and E. Murad, J. Chem. Phys. **93**, 7780 (1990).

39. I. Dotan, A. J. Midey and A. A. Viggiano, J. Am. Soc. Mass Spectrom. **10**, 815 (1999).

40. I. Dotan and W. Lindinger, J. Chem. Phys. **76**, 4972 (1982).

41. R. G. Orth, J. H. Futrell and Y. Nishimura, J. Chem. Phys. **75**, 3345 (1981).

42. I. Dotan, A. J. Midey and A. A. Viggiano, J. Chem. Phys. In press (2000).

43. C. Praxmarer, A. Hansel, W. Lindinger and Z. Herman, J. Chem. Phys. **109**, 4246-4251 (1998).

44. T. Su and W. J. Chesnavich, J. Chem. Phys. **76**, 5183-5185 (1982).

45. T. Su, J. Chem. Phys. **89**, 5355 (1988).

46. D. J. Levandier, R. A. Dressler and E. Murad, Rev. Sci. Instrum. **68**, 64 (1997).

47. D. J. Levandier, R. A. Dressler, S. Williams and E. Murad, J. Chem. Soc. Faraday Trans. **93**, 2611-2617 (1997).

48. S. T. Arnold, A. A. Viggiano and R. A. Morris, J. Phys. Chem. A **102**, 8881 (1998).

49. S. T. Arnold, I. Dotan, S. Williams, A. A. Viggiano and R. A. Morris, J. Phys. Chem. A **104**, 928-934 (2000).

50. F.-S. Huang and R. S. Dunbar, Int. J. of Mass Spectrom. and Ion Process. **109**, 151-170 (1991).

51. P. Ausloos, J. Am. Chem. Soc. **104**, 5259-5265 (1982).

52. W. G. Hwang, J. H. Moon, J. C. Choe and M. S. Kim, J. Phys. Chem. A. **102**, 7512-7518 (1998).

53. R. D. Levine and R. B. Bernstein, *Molecular Reaction Dynamics and Chemical Reactivity* - (Oxford University Press, New York, 1987).

54. S. T. Arnold, J. V. Seeley, J. S. Williamson, P. L. Mundis and A. A. Viggiano, J. Phys. Chem. A **104**, 5511 (2000).

55. I. Dotan, D. L. Albritton and F. C. Fehsenfeld, J. Chem. Phys. **64**, 4334 (1976).

Table 1. Temperature dependent rate constants and collision rate constants for the reactions of $H_3O^+(H_2O)_n$ with acetaldehyde.

Reaction		Rate Constant (10^{-9} cm^3 s^{-1}), [k_c]	
		200 K	294 K
$H_3O^+ + CH_3CHO \rightarrow$	$CH_2OH^+ + H_2O$	4.7 [4.7]	3.7 [3.9]
$H_3O^+(H_2O) + CH_3CHO \rightarrow$	$H_3O^+(CH_2O) + H_2O$	4.1 [3.8]	3.5 [3.2]
$H_3O^+(H_2O)_2 + CH_3CHO \rightarrow$	$H_3O^+(H_2O)(CH_3CHO) + H_2O$	3.7 [3.5]	3.1 [2.9]
$H_3O^+(H_2O)_3 + CH_3CHO \rightarrow$	Products	3.4 [3.3]	2.9 [2.7]
$H_3O^+(H_2O)_4 + CH_3CHO \rightarrow$	Products	3.5 [3.1]	

Table 2. Temperature dependent rate constants, collision rate constants, and product distributions for the reactions of $H_3O^+(H_2O)_n$ with formaldehyde.

| Reaction		Rate Constant (10^{-9} cm^3 s^{-1}), [k_c] Branching Fraction		
		150 K	200 K	294 K
$H_3O^+ + CH_2O \rightarrow$	Products	4.4 [4.9]	3.8 [4.3]	3.3 [3.6]
	$CH_2OH^+ + H_2O$	1.0	1.0	1.0
$H_3O^+(H_2O) + CH_2O \rightarrow$	Products	3.1 [4.1]	2.8 [3.6]	2.3 [3.0]
	$H_3O^+(CH_2O) + H_2O$	1.0	1.0	1.0
$H_3O^+(H_2O)_2 + CH_2O \rightarrow$	Products	2.0 [3.8]	1.6 [3.3]	1.1 [2.8]
	$H_3O^+(H_2O)(CH_2O) + H_2O$	~0.5	1.0	1.0
	$H_3O^+(H_2O)_2(CH_2O)$	~0.5		
$H_3O^+(H_2O)_3 + CH_2O \rightarrow$	Products	1.6 [3.6]	1.2 [3.2]	1.4 [2.7]
	$H_3O^+(H_2O)_2(CH_2O) + H_2O$	~0.5	1.0	1.0
	$H_3O^+(H_2O)_3(CH_2O)$	~0.5		
$H_3O^+(H_2O)_4 + CH_2O \rightarrow$	Products	0.7 [3.5]	1.7 [3.1]	
$H_3O^+(H_2O)_5 + CH_2O \rightarrow$	Products	1.1 [3.5]		

14

Table 3. Rate constants in cm3 s-1 for the reaction of air plasma ions with alkylbenzenes at 298 K as measured in the VT-SIFDT. The collision rate constants have been calculated using the Su-Chesnavich model.[44, 45]

| Ion (Recombination Energy)	Rate Constant, [Collision Rate] (10^{-9} cm^3 s^{-1})		
	Toluene C_7H_8	Ethylbenzene C_8H_{10}	Propylbenzene C_9H_{12}
NO^+ (9.26 eV)	1.6 [1.8]	2.0 [2.0]	2.1 [2.1]
O_2^+ (12.07 eV)	1.7 [1.8]	2.2 [1.9]	1.9 [2.0]
O^+ (13.62 eV)	2.2 [2.3]	2.4 [2.6]	2.6 [2.7]
N^+ (14.53 eV)	2.2 [2.5]	2.6 [2.7]	2.7 [2.8]
N_2^+ (15.58 eV)	1.9 [1.9]	1.9 [2.0]	2.1 [2.1]

Fig. 1. (a) Reaction efficiencies as a function of temperature for the reactions of $H_3O^+(H_2O)_n$ with CH_2O. (b) Reaction efficiencies as a function of cluster size at 150 K, 200 K, and 294 K
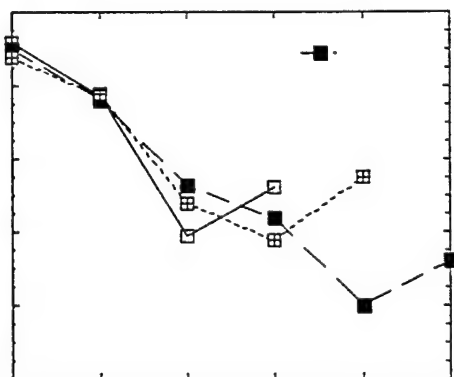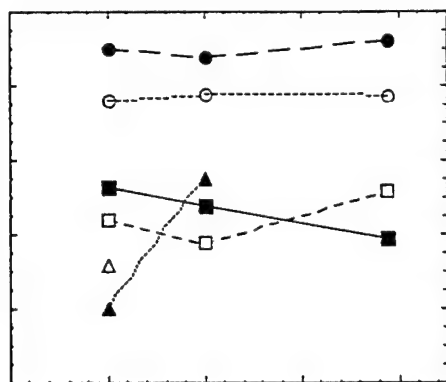
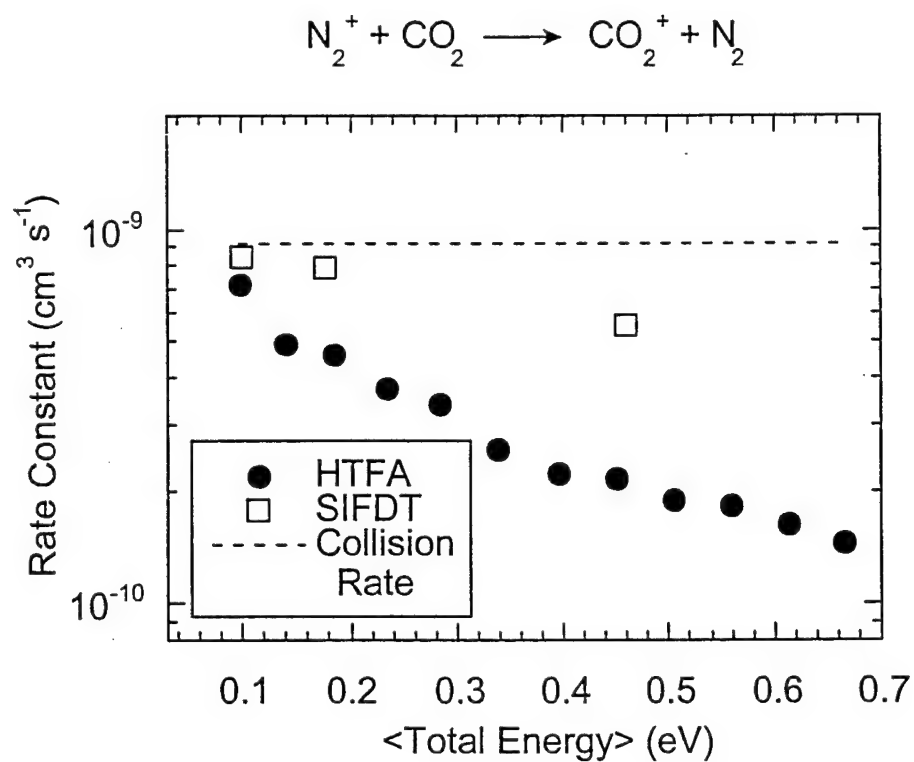**Fig. 2.** Rate constants in cm^3 s^{-1} for the reaction of Cl^- with C_2H_5Br as a function of kinetic energy in eV. Closed and open circles represent the total rate constant and the S_N2 only rate constant at 220 K, respectively. Closed and open squares represent the total rate constant and the S_N2 only rate constant at 298 K, respectively. The pure temperature dependent data of the direct S_N2 reaction is given by triangles with a least squares fit line. The triangles include data at 400 and 500 K where no correction is needed. For the correction at low temperature, see the text. The solid line refers to the study of Caldwell et. al. (CMK).[21] The dashed line refers to the study of Knighton et al. (KBOG).[22] The $\times$ refers to the study of Depuy et al. (DGMB).[20]

$$Cl^- + C_2H_5Br \rightarrow Br^- + C_2H_5Cl$$
$$\rightarrow Cl^-(C_2H_5Br)$$
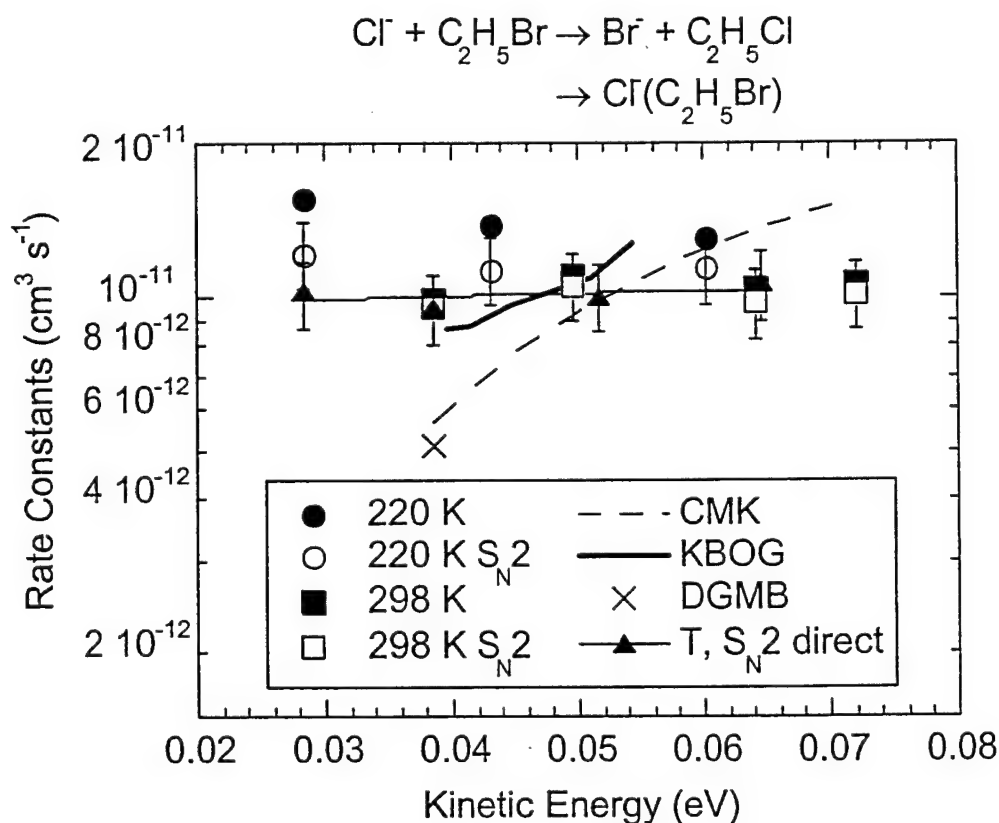
Fig. 3. Rate constants in cm^3 s^{-1} for the reaction of Cl^- with n-C_3H_7Br as a function of kinetic energy in eV. Closed and open circles represent the total rate constant and the S_N2 only rate constant at 230 K, respectively. Closed and open squares represent the total rate constant and the S_N2 only rate constant at 298 K, respectively. The diamonds refer to 500 K data. The × refers to the study of Depuy et al. (DGMB).[20] The point labeled "Direct only" is an upper limit to the direct S_N2 reaction at 230 K. See text for details.
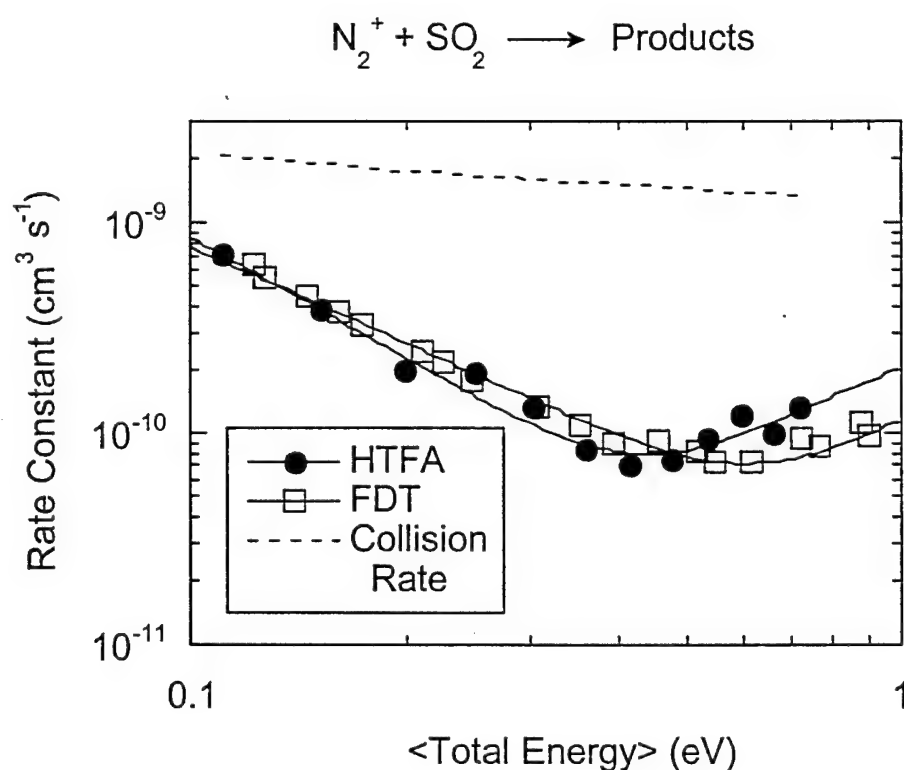

$$Cl^- + C_3H_7Br \rightarrow Br^- + C_3H_7Cl$$
$$\rightarrow Cl^-(C_3H_7Br)$$
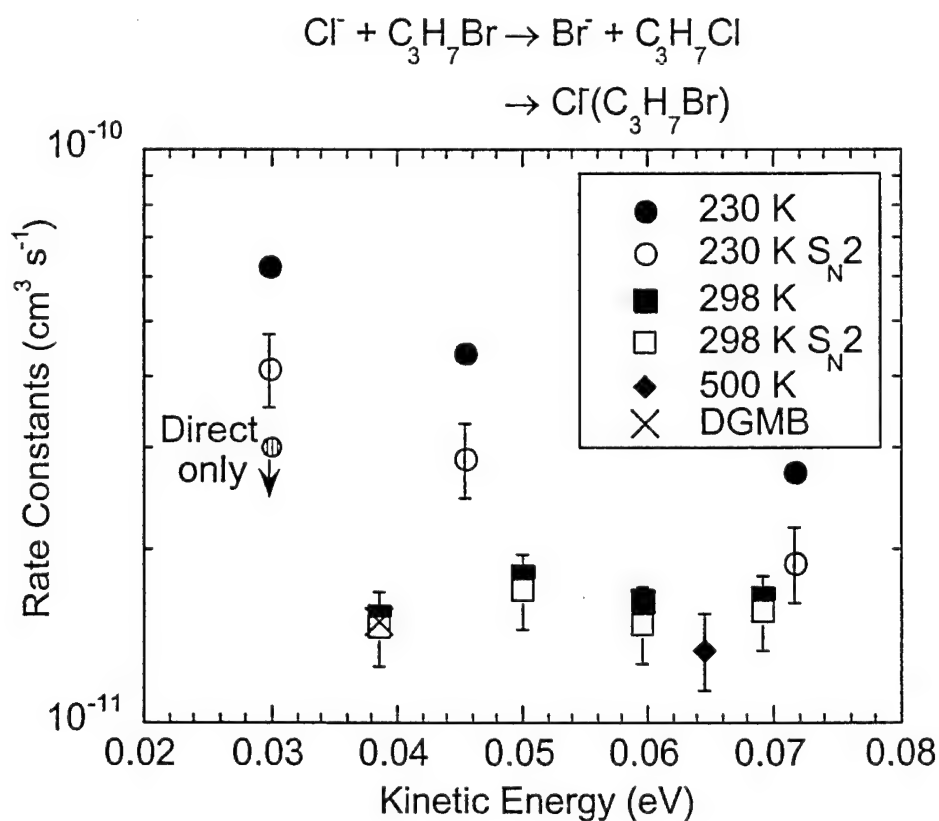
Fig. 4. Rate constants in cm^3 s^{-1} for the reaction of N_2^+ with CO_2 plotted as a function of the average total energy in eV. The solid symbols ($\blacktriangleright$) represent the current HTFA results and the open symbols ($\square$) represent the current SIFDT results at 298 K. The dashed line represents the Langevin collision rate constant.

$$N_2^+ + CO_2 \longrightarrow CO_2^+ + N_2$$

Fig. 5. Rate constants in $cm^3 \, s^{-1}$ for the reaction of N_2^+ with SO_2 plotted as a function of the average total energy in eV. The solid symbols (▶) represent the current HTFA results and the open symbols (□) represent the previous FDT results of Dotan et al. The dashed line represents the Su-Chesnavich collision rate constant.[44, 45] The HTFA rate constants have been multiplied by 1.2 to better overlap with the FDT data. The solid lines are fits to the data using the functional form: $k(E) = A_1(0.111/E)^n + A_2 \exp(-E_a/E)$.

Fig. 6. Rate constants in cm^3 s^{-1} for SO^+ production only for the reaction of $N_2^+ + SO_2$ plotted as a function of the average total energy in eV. The solid symbols (▶) and (■) represent the current HTFA results for the SO_2^+ and SO^+ channels, respectively and the open symbols (○) and (□) represent the previous FDT results of Dotan et al.[55] for the SO_2^+ and SO^+ channels, respectively.

$$N_2^+ + SO_2 \rightarrow SO^+ + O + N_2$$

$$\rightarrow SO_2^+ + N_2$$

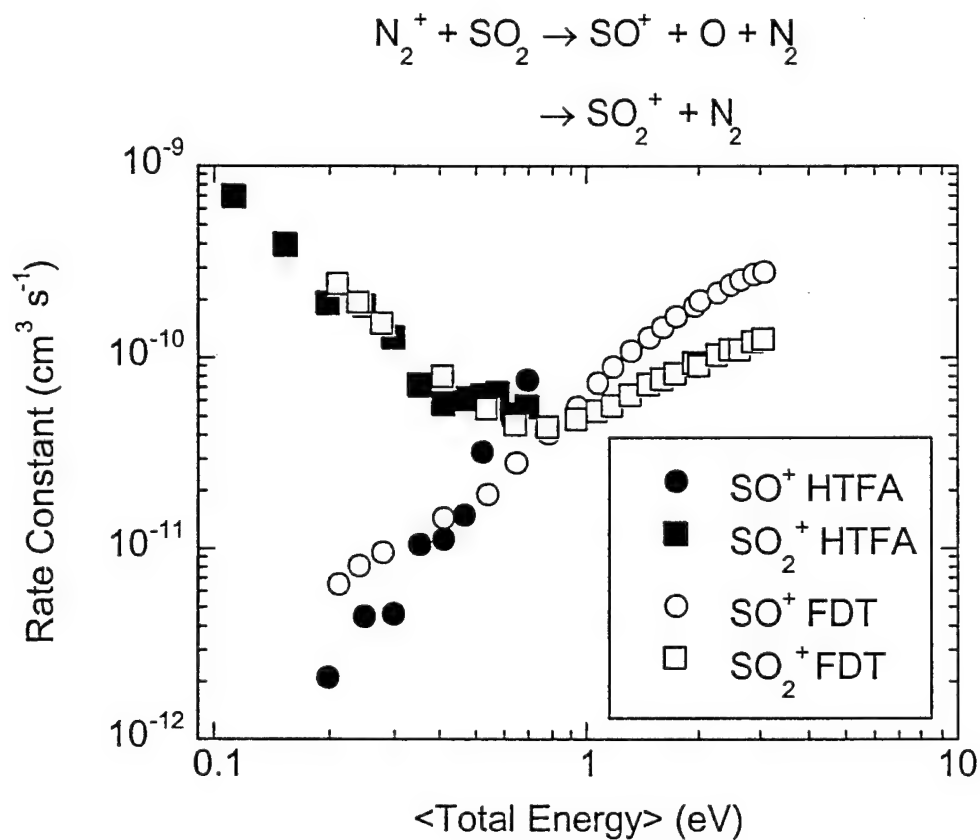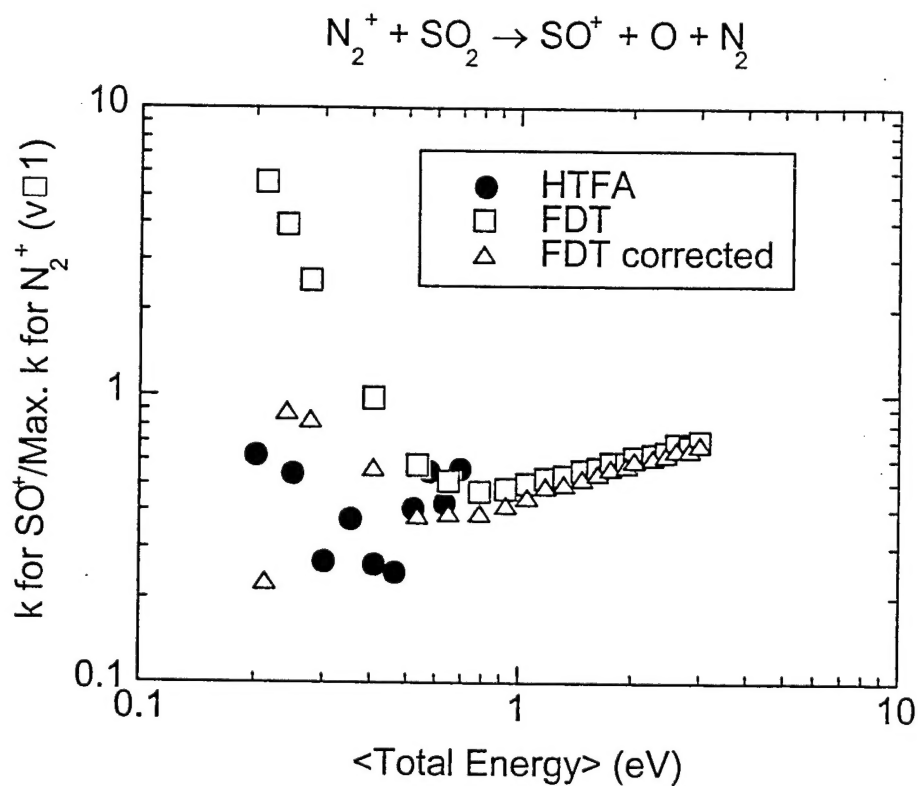**Fig. 7.** Rate constants for the SO^+ channel divided by the maximum rate constant for the reaction of N_2^+ ($v \leq 1$). The N_2^+ ($v \leq 1$) rate is defined as the collision rate constant times the N_2^+ ($v \leq 1$) population. The solid symbols ($\blacktriangleright$) represent the current HTFA results and the open symbols ($\square$) represent the previous FDT results of Dotan et al.[55] The open triangles ($\triangle$) represent the FDT with a background subtracted.

$$N_2^+ + SO_2 \rightarrow SO^+ + O + N_2$$

Legend:
● HTFA
□ FDT
△ FDT corrected

y-axis: k for SO^+/Max. k for N_2^+ ($v \square 1$)

x-axis: <Total Energy> (eV)

Fig. 8 Breakdown diagrams for the reactions of toluene (C_7H_8) with various ions showing (a) $C_7H_8^+$ and (b) $C_7H_7^+$ as a function of total energy. An $\otimes$ symbol marks an
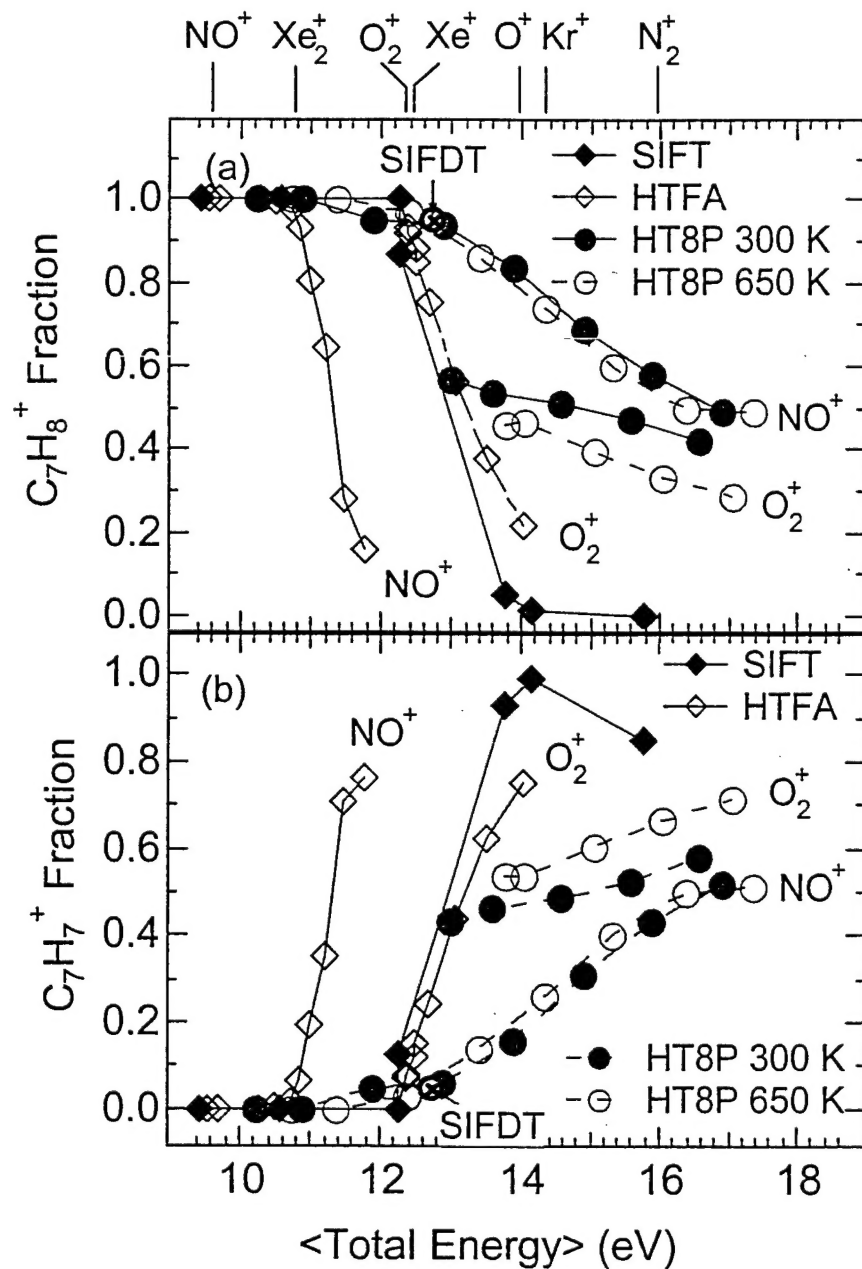
O_2^+ SIFDT result at 300 K with a center-of-mass collision energy of 0.52 eV

Fig. 9 Breakdown diagrams for the reactions of ethylbenzene (C_8H_{10}) with various ions showing (a) $C_8H_{10}^+$ and (b) $C_7H_7^+$ as a function of total energy. An $\otimes$ symbol marks an
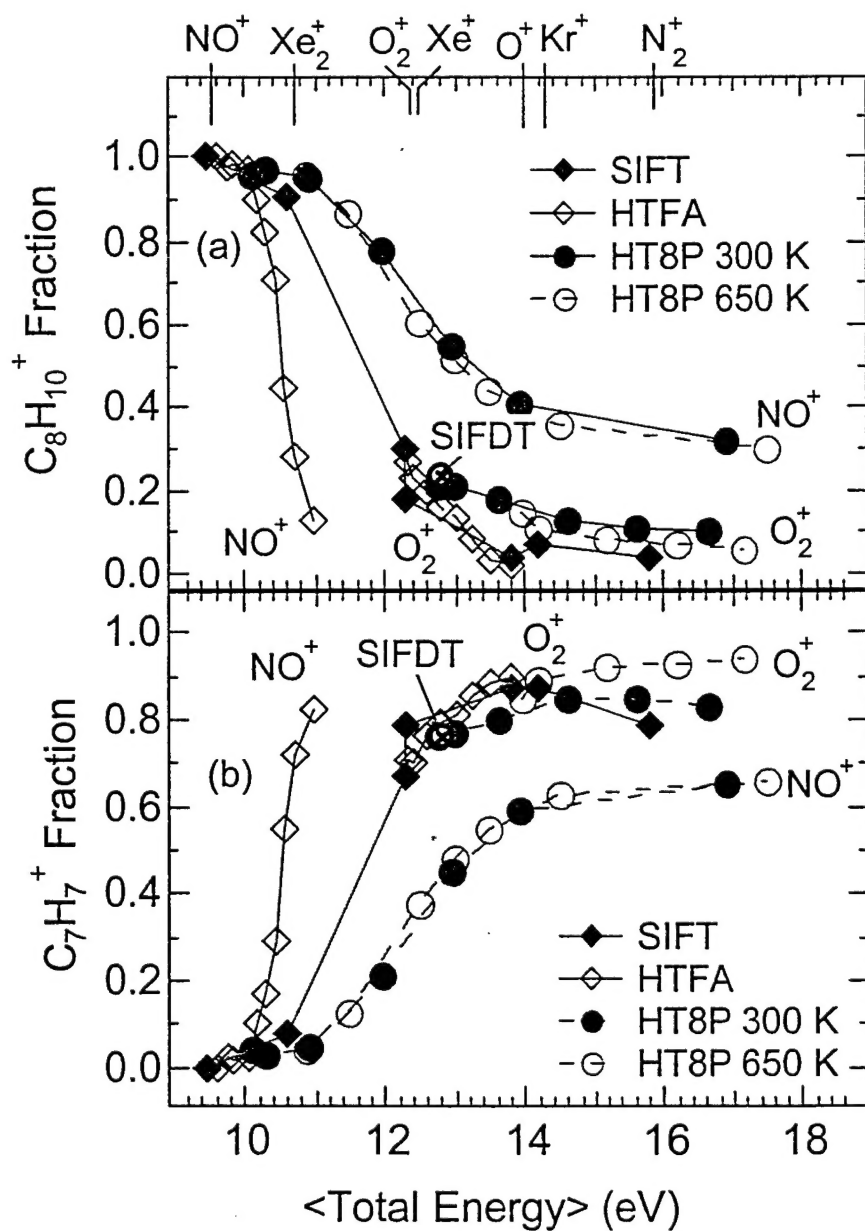
O_2^+ SIFDT result at 300 K with a center-of-mass collision energy of 0.52 eV

Fig. 10 Breakdown diagrams for the reactions of propylbenzene (C_9H_{12}) with various ions showing (a) $C_9H_{12}^+$ and (b) $C_7H_7^+$ as a function of total energy. An $\otimes$ symbol marks an O_2^+ SIFDT result at 300 K with a center-of-mass collision energy of 0.52 eV